



HAL
open science

The effect of water and electron collisions in the rotational excitation of HF in comets

J. Loreau, A Faure, François Lique

► **To cite this version:**

J. Loreau, A Faure, François Lique. The effect of water and electron collisions in the rotational excitation of HF in comets. *Monthly Notices of the Royal Astronomical Society*, 2022, 516, pp.5964-5971. 10.1093/mnras/stac2378 . insu-03860258

HAL Id: insu-03860258

<https://insu.hal.science/insu-03860258>

Submitted on 23 Nov 2022

HAL is a multi-disciplinary open access archive for the deposit and dissemination of scientific research documents, whether they are published or not. The documents may come from teaching and research institutions in France or abroad, or from public or private research centers.

L'archive ouverte pluridisciplinaire **HAL**, est destinée au dépôt et à la diffusion de documents scientifiques de niveau recherche, publiés ou non, émanant des établissements d'enseignement et de recherche français ou étrangers, des laboratoires publics ou privés.

The effect of water and electron collisions in the rotational excitation of HF in comets

J. Loreau¹*, A. Faure² F. Lique³

¹ *KU Leuven, Department of Chemistry, 3001 Leuven, Belgium*

² *Univ. Grenoble Alpes, CNRS, IPAG, F-38000 Grenoble, France*

³ *Université de Rennes 1, F-35042 Rennes, France*

19 August 2022

ABSTRACT

We present the first set of rate coefficients for the rotational excitation of the 7 lowest levels of hydrogen fluoride (HF) induced by collision with water molecules, the dominant collider in cometary comas, in the 5–150 K temperature range. The calculations are performed with a quantum statistical approach from an accurate rigid rotor *ab initio* interaction potential. Rate coefficients for excitation of HF by electron-impact are also computed, within the Born approximation, in the 10 – 10,000 K temperature range. These rate coefficients are then used in a simplified non-local thermodynamic equilibrium (non-LTE) model of a cometary coma that also includes solar radiative pumping and radiative decay. We investigate the range of H₂O densities that lead to non-LTE populations of the rotational levels of HF. We show that to describe the excitation of HF in comets, considering collisions with both water molecules and electrons is needed as a result of the large dipole of HF.

Key words: Comets:general, molecular data, molecular processes, scattering.

1 INTRODUCTION

The interpretation of molecular spectra from astronomical sources is often performed under the assumption of local thermodynamic equilibrium (LTE). However, many astrophysical objects, including the interstellar medium, protoplanetary disks and comets, display non-LTE behaviour due to low particle densities ($n \ll 10^{10} \text{ cm}^{-3}$). An accurate modelling of spectra then requires an understanding of the balance between collision-induced transitions, spontaneous emission and radiatively-induced transitions. Non-LTE radiative transfer models rely on state-to-state rate coefficients for collisional energy transfer that can be computed using a variety of theoretical approaches. In the cometary coma, collisional excitation is generally dominated by collisions with H₂O and electrons and, for comets at large heliocentric distances, by CO (Bockelée-Morvan et al. 2004). While accurate rate coefficients for molecular excitation by collisions with He or H₂ based on quantum-mechanical scattering calculations and *ab initio* interaction potentials have been reported in the literature, data are scarce for excitation induced by H₂O molecules. In that case, the high density of rotational states of both colliders, combined with a deep and anisotropic interaction potential, make fully quantum-mechanical calculations challenging in terms

of computational time and memory requirements. State-to-state rate coefficients for collisional excitation by water molecules are available for only a handful of systems such as H₂O-CO (Green 1993; Faure, Lique & Loreau 2020), H₂O-H₂O (Buffa et al. 2000; Boursier et al. 2020), and H₂O-HCN (Dubernet & Quintas-Sánchez 2019) and have all been obtained with an approximate treatment of the dynamics.

In a recent work, we reported new rate coefficients for H₂O-CO excitation and showed for a generic coma model that the non-LTE regime occurred for H₂O densities in the range $10^3 - 10^8 \text{ cm}^{-3}$ (Faure, Lique & Loreau 2020). Furthermore, we also showed that uncertainties in the collisional data have significant influence on the CO population distribution and that collisions with electrons have a negligible impact except for unrealistically high electron fraction (Faure, Lique & Loreau 2022). The present work focuses on the excitation of hydrogen fluoride by water molecules and electrons. HF is thought to be the main reservoir of fluorine in the interstellar medium (Neufeld & Wolfire 2009), and evidence suggests that in dense molecular clouds, HF is present on the surface of grains rather than in the gas-phase (Phillips et al. 2010; Emprechtinger et al. 2012). HF should thus be present in comets formed from protostellar material. This has been tentatively confirmed by the far-infrared marginal detection of HF in the atmosphere of comet C/2009 P1 Garradd with the *Herschel* Space Observatory (Bockelée-Morvan et al. 2014) and of

* E-mail: jerome.loreau@kuleuven.be

comet 67P/Churyumov-Gerasimenko through *in situ* detection (via mass spectroscopy) with the *Rosetta* spacecraft (Dhooghe et al. 2017). The existence of distributed sources of HF (and other halogen halides) in the form of dust particles in the coma of 67P confirms that it is incorporated in dust grains (De Keyser et al. 2017). As HF is the best candidate to gain insights into the abundance of halogens in comets, it is important to investigate its collisional properties with the most abundant colliders in comas, namely H₂O and free electrons.

In this work we present the first quantum state-to-state rate coefficients for the rotational excitation of HF by H₂O. To that end, we employ a recent *ab initio* potential energy surface combined with a quantum statistical approach. We also use the dipole Born approximation to determine state-to-state rate coefficients for the ro-vibrational excitation of HF by electrons. The computational details are discussed in Section 2 while the HF–H₂O rate coefficients for excitation of the 7 lowest levels of HF are discussed in Section 3. Finally, in Section 4 we illustrate the impact of the new rate coefficients by considering a non-LTE model of the excitation of HF in the cometary coma that includes the effects of collision-induced transitions due to both spin isomers of H₂O (ortho-H₂O and para-H₂O), electrons, radiative pumping of the $v = 0 \rightarrow 1$ band due to solar photons, and radiative decay due to spontaneous emission. We then discuss the relative effects of these sources of (de)excitation. We stress that our objective is not to revisit the HF abundance in comet C/2009 P1 Garradd, which is beyond the scope of this work, but only to evaluate the impact of collisional data on the non-LTE populations of HF. Since HF has similarities with H₂O (mass and dipole moment), we also note that our results should be, at least partly, transferable to the excitation of H₂O in comets. Finally, our main conclusions are drawn in Section 5.

2 HF COLLISIONAL EXCITATION RATE COEFFICIENTS

2.1 HF–H₂O collisions

The calculation of state-to-state rate coefficients for HF–H₂O collisions relies on a recently-reported potential energy surface (PES), on which the scattering is investigated.

2.1.1 Potential energy surface

We employed the high-level *ab initio* PES recently constructed by Loreau et al. (2020). The HF and H₂O colliders were both treated as rigid rotors, with geometrical structures corresponding to their respective ground vibrational state. The interaction energy was calculated on a five-dimensional grid (one distance and four angles) by means of the explicitly-correlated single- and double-excitation coupled cluster theory with a non-iterative perturbative treatment of triple excitations [CCSD(T)-F12a] along with the augmented correlation-consistent aug-cc-pVTZ basis sets. The intermolecular energies were subsequently fitted to a body-fixed expansion expressed as a sum of products of spherical harmonics and a Monte-Carlo estimator was employed to select only the largest expansion terms. This in-

cludes in particular a description of the long-range, which is required to compute collisional excitation rate coefficients at low temperature.

The global minimum of the HF–H₂O PES occurs at a center-of-mass separation of $R = 4.99 a_0$ and corresponds to a non-planar equilibrium structure in which a hydrogen bond is formed with the water molecule acting as proton acceptor. The depth of the PES at the global minimum is $D_e = 3059 \text{ cm}^{-1}$, while the dissociation energy of the molecular complex is $D_0 = 2089.4 \text{ cm}^{-1}$ for o-H₂O–HF and $D_0 = 2079.6 \text{ cm}^{-1}$ for p-H₂O–HF. Full details about the potential surface calculations can be found in the paper by Loreau et al. (2020). We note that recently a new HF–H₂O PES has been presented by Viglaska et al. (2022) for non-rigid monomers and it was found very similar to the PES used in the present work.

2.1.2 HF–H₂O excitation rate coefficients

The most accurate method to compute collisional excitation cross sections and rate coefficients is the quantum-mechanical close-coupling method. However, when the PES on which the collision proceeds has a deep well and/or when the colliders have small rotational constants, the large number of equations that need to be solved simultaneously in order to reach convergence becomes prohibitive. In the present case, we found it impossible to converge close-coupling calculations even for a total angular momentum $J = 0$, so that an alternative approach was required. We rely here on a statistical approach of the dynamics based on a global *ab initio* PES (Loreau, Lique & Faure 2018). The validity of this method, inspired by the statistical adiabatic model of Quack & Troe (1975), has been explored for several systems including H₂O–CO (Loreau, Faure & Lique 2018). It is expected to provide state-to-state rate coefficients that are correct within a factor of 2 for collisions that proceed through a deep well and at relatively low temperature, when the lifetime of the complex is sufficiently long (Konings et al. 2021; Balança et al. 2020).

The statistical method has been described for H₂O–CO collisions elsewhere (Faure, Lique & Loreau 2020) and is applicable to H₂O–HF, so that we only recall its main features here. The angular momenta of the two colliding molecules (\mathbf{j}_1 for H₂O and \mathbf{j}_2 for HF) are coupled to the angular momentum of the relative motion ℓ to form the total angular momentum $\mathbf{J} = \mathbf{j}_1 + \mathbf{j}_2 + \ell$. The interaction Hamiltonian excluding the kinetic term is then diagonalized in a basis of rotational functions for the two colliding molecules. For each value of the total angular momentum J , this leads to a set of adiabatic rotational curves as a function of the intermolecular distance R that can be connected asymptotically to the various rotational states of the molecules. The collision is assumed to take place only if the collision energy is larger than the height of the barrier in the adiabatic curve corresponding to the initial state. The probability is then divided equally among the channels for which the energy is larger than their respective centrifugal barriers, which allows one to compute state-to-state cross sections. These are then integrated over a Maxwell-Boltzmann distribution of energies to obtain rate coefficients.

The cross sections were calculated for transitions between all rotational levels of both o-H₂O and p-H₂O up to

$j_1 = 6$ and HF up to $j_2 = 6$ and for total energies between 0 and 1500 cm^{-1} in order to calculate rate coefficients up to $T = 150 \text{ K}$. The basis set of angular functions included levels up to $j_1 = 9$ and $j_2 = 10$, and tests were performed to ensure the convergence of the results with respect to the size of the basis set of rotational functions. The rotational constant of HF corresponding to the ground vibrational level was taken to be $B_0 = 20.5567 \text{ cm}^{-1}$ (Webb & Narahari Rao 1968), while the energy $E_{j_1 k_a k_c}$ of the rotational levels of H_2O was obtained using the effective Hamiltonian of Kyrö (1981). They are labeled with j_1 , k_a , and k_c , where k_a and k_c are pseudoquantum numbers corresponding to the projection of the angular momentum j_1 along the axis of least and greatest moment of inertia, respectively. Convergence of the cross sections was obtained when considering a maximum value of the total angular momentum $J = 150$. Adiabatic curves were generated for o- H_2O -HF and p- H_2O -HF separately. Indeed, o- H_2O and p- H_2O colliders behave as two different species as they are not connected through inelastic collisions.

Since, in the present work, we are only interested in the excitation of HF, we summed the state-to-state rate coefficients over all possible final states of H_2O and averaged over the initial rotational states of H_2O assuming a thermal population distribution,

$$k_{j_2 \rightarrow j'_2}(T) = \sum_{j_1 k_a k_c j'_1 k'_a k'_c} P_{j_1 k_a k_c}(T) k_{j_1 k_a k_c, j_2 \rightarrow j'_1 k'_a k'_c, j'_2}(T) \quad (1)$$

$$P_{j_1 k_a k_c}(T) = \frac{g_{j_1 k_a k_c} \exp(-E_{j_1 k_a k_c}/k_B T)}{\sum_{j_1 k_a k_c} g_{j_1 k_a k_c} \exp(-E_{j_1 k_a k_c}/k_B T)} \quad (2)$$

where k_B is the Boltzmann constant and g_{j_1} is the level degeneracy. This set of “thermalized” rate coefficients for (de-)excitation of HF assumes that the kinetic and H_2O rotational temperatures are equal, and satisfies detailed balance. At the lowest temperature considered here (10 K) the main contribution to the thermalized rate coefficients originates from excitation by ground state H_2O ($j_{k_a k_c} = 0_{00}$ for p- H_2O and 1_{01} for o- H_2O , respectively) while at higher temperatures the excited rotational states of H_2O dominate.

2.2 HF–electron collisions

Scattering calculations for electron-HF collisions were performed within the dipole Born approximation, which is briefly presented below. We note that this approximation is employed in many models treating excitation of molecules in comets (e.g. Zakharov et al. 2007).

2.2.1 The dipolar Born approximation

Because HF has a strong dipole (1.83 D), dipole-allowed rotational transitions ($\Delta j_2 = \pm 1$) have very large cross sections, especially at low energy (below 1 eV). These cross sections are dominated by high-partial waves, i.e. long-range interactions, so that the dipole Born approximation is expected to be reliable.

The dipole Born integral cross section for a rotational excitation $j_2 \rightarrow j'_2$ can be formulated as follows (Itikawa

1972):

$$\sigma_{j_2 \rightarrow j'_2} = \frac{8\pi}{3k^2} d^2 \frac{S(j_2, j'_2)}{2j_2 + 1} \ln \left| \frac{k + k'}{k - k'} \right|, \quad (3)$$

where k and k' are the initial and final wave numbers of the electron, respectively, d is the permanent dipole moment and the angular factor (or line strength) $S(j_2, j'_2)$ is related to the Einstein coefficient $A_{j'_2 \rightarrow j_2}$ through:

$$A_{j'_2 \rightarrow j_2} = \frac{64\pi^4 \nu^3}{3hc^3} d^2 \frac{S(j_2, j'_2)}{2j'_2 + 1}, \quad (4)$$

where h is the Planck’s constant, c is the speed of light and ν is the frequency of the transition $j_2 \rightarrow j'_2$. The Born rotational cross section can thus be reformulated as:

$$\sigma_{j_2 \rightarrow j'_2} = \frac{hc^3}{8k^2 \pi^3 \nu^3} \frac{(2j'_2 + 1)}{(2j_2 + 1)} A_{j'_2 \rightarrow j_2} \ln \left| \frac{k + k'}{k - k'} \right|. \quad (5)$$

The equation is strictly similar for a ro-vibrational excitation $v_2 j_2 \rightarrow v'_2 j'_2$. In practice, Einstein coefficients were extracted from the HITRAN database (Gordon et al. 2017) for dipole-allowed transitions among all levels below $v_2 = 2$, $j_2 = 0$ which opens at 7750.8 cm^{-1} , i.e. the lowest 34 levels (up to $v_2 = 0$, $j_2 = 19$).

For the rotational excitation of HF, Thummel, Nesbet & Peyerimhoff (1992) have performed high-level calculations by using the variational R -matrix method combined with the frame-transformation theory. They have shown for the excitation $j_2 = 0 \rightarrow 1$ that the Born rotational cross sections are accurate to within a factor of 2 or better, as expected from the large dipole. Good agreement between the Born approximation and experimental rotational cross section for $j_2 = 0 \rightarrow 1$ was also emphasized by Itikawa (2017).

The vibrational excitation of HF was also studied experimentally and theoretically (Itikawa 2017). Strong threshold resonances in the $v_2 = 0 \rightarrow 1$ cross section were soon attributed to short-lived negative-ion states (Rohr & Linder 1976). Indeed, the dipole Born vibrational cross section was found to be about an order of magnitude smaller than the measured cross section (a few \AA^2 at threshold), suggesting that the process is dominated by low-partial waves. We also found a small $v_2 = 0 \rightarrow 1$ Born cross section with a peak of $\sim 0.1 \text{ \AA}^2$ around 1 eV. As a result, our Born cross sections were multiplied by a factor of 10 so that the recommended $v_2 = 0 \rightarrow 1$ cross sections of Itikawa (2017) were reproduced to within a factor of 2 beyond the threshold peak.

2.2.2 HF-electron ro-vibrational rate coefficients

Born cross sections were computed for electron energies up to 9 eV and for all 59 dipole-allowed transitions $v_2 j_2 \rightarrow v'_2 j'_2$. Rate coefficients were deduced by integrating the cross sections over Maxwell-Boltzmann distribution of energies for kinetic temperatures between 10 and 10,000 K. For pure rotational excitation, our rate coefficients should be accurate to better than a factor of 2 while for ro-vibrational excitation their accuracy is expected to be a factor of a few. Better accuracies require higher-level treatments, including short-range effects, such as R -matrix based calculations (see e.g. Ayouz et al. 2021). We note, however, that electron-impact vibrational excitation play a negligible role in the application to comets presented below.

3 RESULTS AND COMPARISON OF COLLISION DATA SETS

Rate coefficients for the rotational de-excitation of HF($j_2 = 1 - 5 \rightarrow j'_2 = 0$) by H₂O are illustrated in Fig. 1 for temperatures of 30 K and 100 K. The dominant de-excitation rates occur for $j_2 = 1$ with values larger than 10^{-10} cm³ s⁻¹, and the de-excitation rate coefficients decrease as Δj_2 increases. At $T = 30$ K the large spacing between energy levels of HF lead to rate coefficients that decrease very quickly as j_2 increases. This observation remains true at $T = 100$ K, although the decrease with increasing j_2 is slightly less marked. The rotational excitation of HF by H₂O depends on two counteracting factors: the PES is deep and anisotropic, which should lead to large excitation rate coefficients; however this is compensated by the large rotational constant of HF. At both temperatures we observe very little differences between the excitation by p-H₂O and o-H₂O, which suggests that the ortho-to-para ratio (OPR) of H₂O should not play a major role in the excitation of HF, similar to what we reported for the excitation of CO by H₂O (Faure, Lique & Loreau 2020).

For comparison, we display in Fig. 2 the rate coefficients for (de-)excitation from the level $j_2 = 2$. At both 30 K and 100 K the dominant transition is the de-excitation towards $j'_2 = 1$, followed by the $j_2 = 2 \rightarrow 0$ transition, while the excitation rate coefficients quickly decrease with increasing j'_2 due to large rotational spacing.

In Figs. 1 and 2, we also compare our results to the data used by Bockelée-Morvan et al. (2014) (hereafter denoted as B14) for the excitation of various molecules, including HF, by H₂O. The B14 rate coefficients were obtained assuming a total cross section $\sigma = 5 \times 10^{-14}$ cm², a value derived from line broadening measurements on H₂O-H₂O. The total collisional rate coefficient was computed as $k(T) = \sigma \langle v(T) \rangle$, where T is the kinetic temperature and $\langle v(T) \rangle$ is the thermal mean velocity of the HF targets relative to the H₂O projectiles. State-to-state rate coefficients $k_{j_2 \rightarrow j'_2}(T)$ were then obtained as $k_{j_2 \rightarrow j'_2}(T) = k(T) P_{j'_2}(T)$, where $P_{j'_2}(T)$ is the Boltzmann population of the final level j'_2 at temperature T (Bockelée-Morvan 1987). This is equivalent to assuming that collisions redistribute the molecule according to the Boltzmann distribution at a temperature given by the kinetic temperature.

For both temperatures presented in Fig. 1 the B14 rate coefficients are much larger than those obtained in the present work. For de-excitation transitions to a given rotational level such as $j_2 \rightarrow j'_2 = 0$, the difference between the two sets of rate coefficients increases with j_2 since the B14 data depend only on the final level j'_2 but not on the initial level j_2 , while the present results suggest a strong decrease with increasing Δj_2 . For transitions $j_2 \rightarrow j'_2 = 0$, this leads to discrepancies of a factor 5 (resp. 4) for $j_2 = 1$ at $T = 30$ K (resp. 100 K) which increases with j_2 to reach a factor 26 (resp. 18) for $j_2 = 4$ at $T = 30$ K (resp. 100 K). For transitions $j_2 = 2 \rightarrow j'_2$ at $T = 100$ K the trends in j'_2 agree between the two sets of results, with the B14 rates coefficients being larger by a factor 3-7 depending on j'_2 . On the other hand, at $T = 30$ K we observe large discrepancies as the B14 rate coefficients are larger than those computed here for HF de-excitation transitions, but smaller for transitions leading to excitation of HF. In addition, at low temperatures

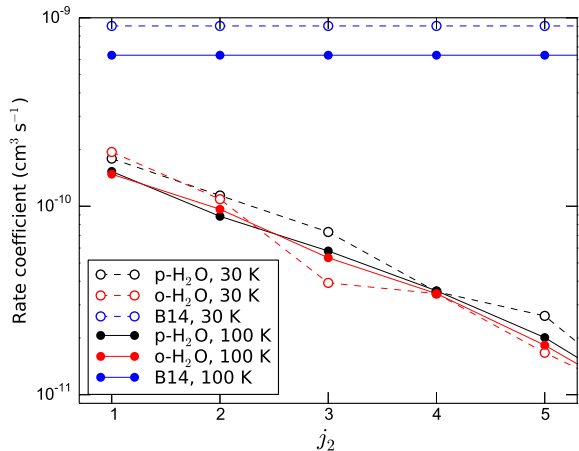


Figure 1. Rate coefficients for the rotational de-excitation of HF($j_2 = 1 - 5 \rightarrow j'_2 = 0$) by H₂O. The projectiles p-H₂O and o-H₂O are assumed to be thermalized at the kinetic temperature (30 or 100 K). The data obtained in the present work is compared to that used by Bockelée-Morvan et al. (2014), denoted as B14.

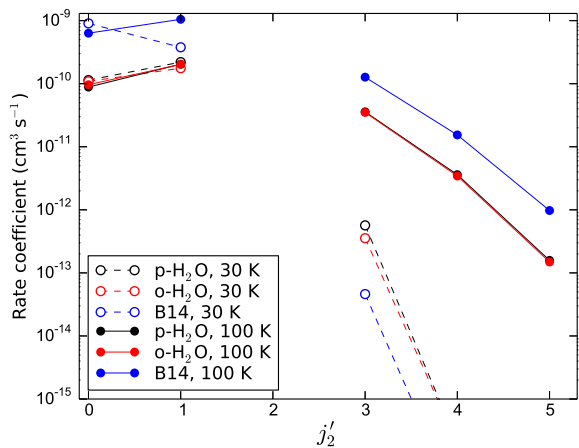


Figure 2. Rate coefficients for the rotational excitation and de-excitation of HF($j_2 = 2 \rightarrow j'_2$).

(e.g., 30 K) our results predict a larger rate coefficient for the HF($2 \rightarrow 1$) transition than for HF($2 \rightarrow 0$), while the reverse is predicted by the B14 data since those rate coefficients only depend on the thermal population of the final state, which is larger for $j_2 = 0$ than $j_2 = 1$ at 30 K.

It is also instructive to compare the (de-)excitation of HF by other colliders. Data is available for the (de-)excitation by p-H₂ and o-H₂ (Guillon & Stoecklin 2012), He (Reese, C. et al. 2005), and H (Desrousseaux & Lique 2018). These data were all obtained with the fully quantum-mechanical close-coupling method based on accurate *ab initio* PESs. The comparison for transitions $j_2 \rightarrow j'_2 = 0$ is shown in Fig. 3 at two temperatures, 30 K and 100 K. With the exception of He, the rate coefficients corresponding to the de-excitation $j_2 = 1 \rightarrow 0$ are of similar magnitude for all colliders. At 30 K the largest difference occurs for de-excitation by o-H₂, with a rate coefficient that is a factor ~ 2 smaller than for de-excitation by H₂O. At 100 K the

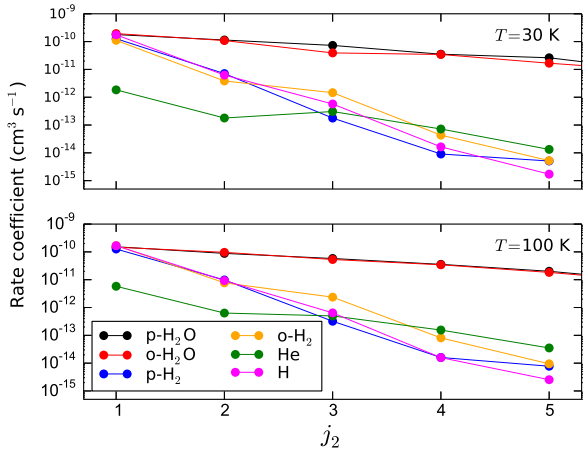


Figure 3. Rate coefficients for the rotational de-excitation of HF($j_2 = 1 - 5 \rightarrow j_2 = 0$) by H₂O at two temperatures (30 K and 100 K), compared to the rate coefficients for de-excitation by collisions with H, He, p-H₂, and o-H₂.

$j_2 = 1 \rightarrow 0$ rate coefficients for the various colliders besides He agree within 20%, the largest difference occurring now for the de-excitation by p-H₂. On the other hand, for the (de-)excitation towards/from more excited rotational levels ($\Delta j_2 > 1$) we observe that H₂O is a much more efficient collider, with differences of up to two orders of magnitude for the $j_2 = 3 \rightarrow 0$ transition. This slower decrease of the rate coefficients with increasing Δj_2 is a direct consequence of the deeper well and large anisotropy of the HF–H₂O PES compared to the other systems (the well depth D_e of the H₂O–HF complex is 3059 cm⁻¹, while it is 359 cm⁻¹ for HF–H₂, 135 cm⁻¹ for HF–H₂, and 43.7 cm⁻¹ for HF–He).

The rate coefficients for de-excitation by electron impact are shown in Fig. 4 for dipolar transitions $j_2 \rightarrow j_2 - 1$ for temperatures between 10 K and 10⁴ K. The large dipole moment of HF leads to rate coefficients that are in excess of 10⁻⁷ cm³s⁻¹ for all temperatures. At the lowest temperature (10 K) we observe a strong dependence of the rate coefficients on the initial value of j_2 . This dependence decreases with increasing temperature to become almost negligible at $T = 10^4$ K.

All de-excitation rate coefficients are available as supplementary material and will be made available, along with the spectroscopic data, in the EMAA database at <http://emaa.osug.fr> and in the LAMDA database at <https://home.strw.leidenuniv.nl/moldata/>. Excitation rate coefficients can be derived using the detailed balance principle.

4 NON-LTE MODEL OF HF IN COMETS

To assess the impact of the new collisional rate coefficients, we use here the same non-LTE model of a cometary coma as in Faure, Lique & Loreau (2020). We compute the rotational level population of HF based on a generic model of the coma that is not representative of a particular comet. The comet is assumed to be located at a distance of 1 au from the Sun, with a total production rate $Q_{\text{H}_2\text{O}} = 10^{29}$ s⁻¹, an expansion velocity $v_{\text{exp}} = 0.8$ km s⁻¹, and a uniform

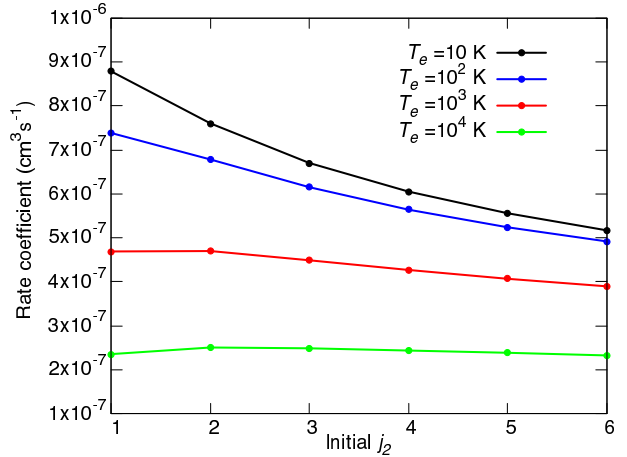


Figure 4. Rate coefficients for the rotational de-excitation $j_2 \rightarrow j_2 - 1$ of HF by electrons at four temperatures (10 K, 100 K, 1000 K, and 10000 K).

neutral gas temperature. Furthermore, we assume that the collisional (de-)excitation of HF is due to both H₂O and electrons, and that the water density profile follows a spherical Haser model (as illustrated in Fig. A1).

For the electron density and temperature radial profiles, we use the model described by Zakharov et al. (2007) where full details can be found. The scaling factor x_{ne} for the electron density is used as a free parameter (see their Eq. 5). We note that the default value $x_{ne} = 1$ was derived from Giotto measurements in comet 1P/Halley. Electron temperature and density profiles are shown in Fig. A1. As in the model used by Zakharov et al. (2007), the electron temperature is fixed to the gas kinetic temperature for $R < R_{cs}$ and it increases linearly with R up to $R = 2R_{cs}$, where it reaches its maximum value of $T = 10^4$ K. R_{cs} is the distance of the ‘contact’ surface (separating the purely cometary plasma from the region containing solar wind charged particles) and where R_{rec} is the distance of the ‘recombination’ surface (outside which the recombination rate of electrons with ions is negligible). We note that the bump in the electron density can be partly attributed to the decrease of the recombination rate of electrons with ions caused by the strong increase of the electron temperature.

The coupled radiative transfer and statistical equilibrium (SE) equations are solved with the public version of the RADEX escape probability code, using the large velocity gradient (LVG) approximation. In its public version, the electron and neutral temperatures are identical. We have therefore implemented in RADEX an electron temperature that can differ from the H₂O kinetic temperature. The radiative transfer is treated as both local and steady-state by running a grid of RADEX calculations covering a range of H₂O densities (see below). We thus assume that time-dependent effects are negligible and we also ignore HF photodissociation (including photoionization). These two approximations can be assessed by comparing the relative importance of the different rates on the HF level population. As shown in Fig. A2 for the HF level $j_2 = 1$, in the inner coma, collisions with water molecules are largely dominant while in the outer coma, the radiative processes (mainly the spontaneous emission $j_2 = 1 \rightarrow 0$) become the most important. In the intermedi-

ate region between 10^2 km and 10^4 km, the contribution of electron collisions is also significant. On the other hand, the photodissociation and expansion rates have both a minor contribution over the entire coma. As a result, both photochemical and time-dependent effects should have a negligible impact on the HF populations and the usual steady-state assumption of SE is expected to be reliable (see details in Appendix A).

The input parameters to RADEX are the kinetic temperature, T_k , the column density of HF, $N(\text{HF})$, the line width, Δv , and the density of the colliders, here $n_{\text{H}_2\text{O}}$ and n_e . A representative kinetic temperature of 50 K was chosen. The column density was fixed at $N(\text{HF}) = 10^{11} \text{ cm}^{-2}$, which is the typical magnitude at $r \sim 1000$ km for a HF/H₂O abundance ratio of $\sim 1.8 \times 10^{-4}$ (Bockelée-Morvan et al. 2014). This column density corresponds to line opacities lower than 0.1. The background radiation field includes both the 2.73 K cosmic microwave background (CMB) (of negligible importance) and the Sun radiation. Other parameters are taken as in Faure, Lique & Loreau (2020), where details are provided.

Input data include the HF energy levels (v_2, j_2) , the spontaneous emission Einstein coefficients and the collisional rate coefficients. Level energies and Einstein coefficients were taken from the HITRAN database, as for the electron-impact excitation calculations described above. Only the first excited vibrational level $v_2 = 1$ was taken into account. Our model thus include the lowest 34 ro-vibrational levels of HF, i.e. up to level $(0, 19)$ which lies 7515.3 cm^{-1} above the ground-state $(0, 0)$. Since our H₂O-HF SACM rate coefficients are available for the lowest 7 rotational levels only, we had to extrapolate the H₂O-HF collisional data above $j_2 = 6$. The method implemented by Faure, Lique & Loreau (2020) for H₂O-CO was employed here for H₂O-HF. It should be noted, however, that the corresponding levels are negligibly populated (less than 1%) over the entire coma so that the extrapolated collisional data play a negligible role in the SE equations.

In a first instance we consider only excitation by H₂O and neglect the contribution of electrons by setting $x_{n_e} = 0$. The population of HF levels j_2 obtained with our non-LTE model based on the set of thermalized SACM rate coefficient is plotted as a function of the H₂O density in Fig. 5 for a kinetic temperature of 50 K and with an OPR for H₂O set to 3. We can clearly observe the presence of three different regimes: the fluorescence equilibrium at low densities ($n_{\text{H}_2\text{O}} \lesssim 10^5 \text{ cm}^{-3}$), the non-LTE regime in the range $10^5 \lesssim n_{\text{H}_2\text{O}} \lesssim 10^{10} \text{ cm}^{-3}$ and the LTE-regime at larger densities. Based on the isotropic Haser model and a production rate $Q_{\text{H}_2\text{O}} = 10^{29} \text{ s}^{-1}$, this implies that LTE applies for HF at $r \lesssim 30$ km, i.e. in the inner coma, while the fluorescence equilibrium distribution is completely established at $r \gtrsim 10^4$ km (see Fig. A1). The non-LTE regime thus extends typically from 30 to 10,000 km. This can be compared to the collisional excitation of CO, for which the non-LTE regime extends from 300 to 70,000 km (corresponding to $10^3 \lesssim n_{\text{H}_2\text{O}} \lesssim 10^8 \text{ cm}^{-3}$) for identical coma parameters (Faure, Lique & Loreau 2020). This difference mainly reflects the larger spontaneous emission rates in HF. We note that in the fluorescence equilibrium regime, only the ground rotational state of HF is significantly populated at a kinetic temperature of 50 K (the population of $j_2 = 1$ is

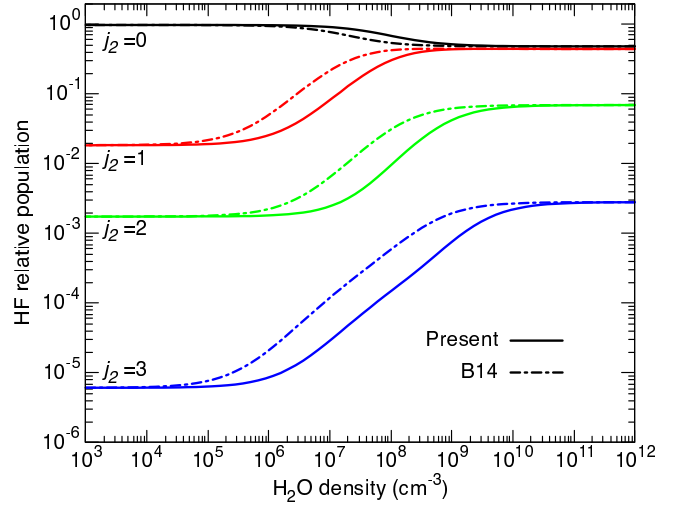


Figure 5. Level populations of HF ($j = 0-3$) as functions of H₂O density for our non-LTE model at a temperature of 50 K. Two sets of collisional data for H₂O collisions are employed: the thermalized SACM set with the OPR of H₂O fixed at 3 (solid lines) and the B14 set (dashed lines). Electron collisions are neglected by setting $x_{n_e} = 0$. See text for details.

about 2%), while at thermal equilibrium the population of the $j_2 = 0 - 2$ levels is 48%, 44%, and 7%, respectively.

On Fig. 5 we also show the rotational population obtained with the B14 set of rate coefficients. Since the rate coefficients computed in this work are smaller than those of (Bockelée-Morvan et al. 2014), one of the main differences between the two sets of data is that the LTE equilibrium is predicted to be reached at H₂O densities almost one order of magnitude higher than if the B14 rate coefficients are employed. The population of ground state HF ($j_2 = 0$) is also predicted to be higher than with the B14 set, while the population of excited rotational states is smaller by up to a factor 3. A similar effect was observed for the excitation of CO by H₂O (Faure, Lique & Loreau 2020).

We now consider the impact of excitation by electrons. The population of the HF rotational levels including excitation by electron-impact is shown in Fig. 6. It can be seen that electrons play a major role for HF at H₂O densities around $5 \times 10^6 \text{ cm}^{-3}$, leading to a decrease of the population of the ground state $j_2 = 0$ and a strong increase of the population of excited rotational states. The largest impact occurs due to the jump in electron density at a distance of about 2000 km from the comet nucleus (see Fig. A1). We conclude that electron-impact excitation play a significant role, even for a standard i.e. moderate value of the scaling factor ($x_{n_e} = 1$). The importance of electron collisions for polar species was indeed emphasized in previous works (Xie & Mumma 1992). This again supports the need for higher-level electron-HF calculations in order to confirm, and possibly improve, the present results.

Regarding the (marginal) detection of HF $j_2 = 1 \rightarrow 0$ in comet C/2009 P1 (Garradd) with Herschel (Bockelée-Morvan et al. 2014), our results show that using the SACM HF-H₂O rate coefficients will require a larger HF abundance than using the B14 rate coefficients, whatever the excitation model. Indeed, as plotted in Figure 5, the population of $j_2 = 1$ is significantly reduced at interme-

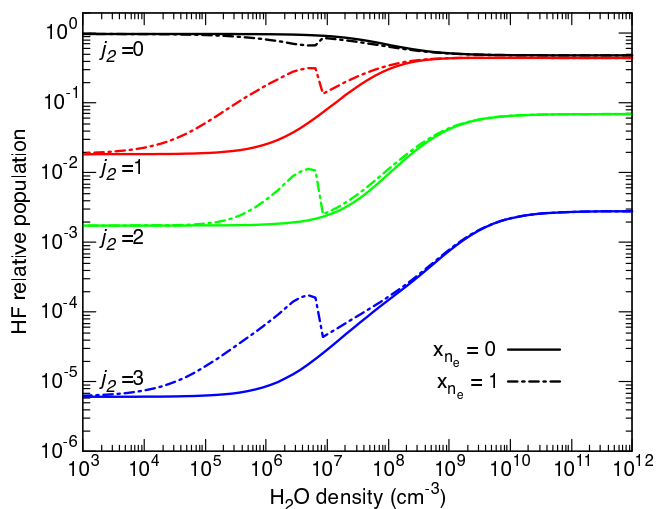


Figure 6. Level populations of HF ($j = 0 - 3$) as functions of H_2O density for our non-LTE model. The collisional data are the thermalized SACM rate coefficients for H_2O collisions with the OPR of H_2O fixed at 3 (solid lines) complemented with the Born rate coefficients for electron collisions (dot-dashed lines). The scaling factor x_{n_e} is taken equal to 1. See text for details.

diate densities when the present (smaller) rate coefficients are employed. Of course the actual impact of the new rate coefficients depends on the contribution of the intermediate density region to the overall flux within the Herschel beam. It thus depends on the exact physical model used for C/2009 P1 and, in particular, on the gas temperature profile which was taken as variable in Bockelée-Morvan et al. (2014). Such a detailed modeling is clearly beyond the scope of this work, but our results suggest that the HF/ H_2O abundance ratio ($1.8 \pm 0.5 \times 10^{-4}$) derived by Bockelée-Morvan et al. (2014) and used as a proxy for the F/O elemental ratio is a lower limit. Within the uncertainty margins, it may still be consistent with values derived for other Solar System objects (see Table 3 in Dhooghe et al. (2017)), in particular the F/O ratio measured with *Rosetta* in comet 67P which varies between $0.2 - 4 \times 10^{-4}$, with a weighted average bulk value of 0.89×10^{-4} . Clearly, only a future far-IR observatory in space or at airborne altitude will be able to confirm or refute the identification of HF in comet C/2009 P1. If confirmed, the present set of SACM collisional data will be essential to derive an accurate F/O ratio.

5 CONCLUDING REMARKS

In this work we obtained the first quantum state-to-state rate coefficients corresponding to the rotational excitation of HF by p- H_2O and o- H_2O for temperatures up to 150 K and rotational levels up to $j_2 = 6$. The calculations were performed by means of a quantum statistical approach based on a recent five-dimensional *ab initio* potential energy surface obtained from highly correlated approaches.

The state-to-state rate coefficients were summed over the final states of H_2O and averaged over the initial rotational states of H_2O assuming a rotational population corresponding to equilibrium at the kinetic temperature to provide thermalized rate coefficients. The comparison with ap-

proximate data calculated in previous works using simple assumptions showed large differences at all temperatures considered. We also found H_2O to be a more efficient collider than H_2 , H, or He in the excitation of HF, and the excitation by o- H_2O or p- H_2O to be very similar.

The data were then used in a generic non-LTE model of the cometary coma. We showed that the rotational population of HF is strongly affected by collisional excitation for H_2O densities in the range between 10^5 cm^{-3} and 10^{10} cm^{-3} .

Moreover, we provided rate coefficients for the excitation of HF by electron in the Born approximation. The corresponding rate coefficients were found to be large ($> 10^{-7} \text{ cm}^3 \text{ s}^{-1}$) as a result of the large dipole moment of HF. This suggests that electrons will compete with neutrals in exciting HF when the electron-to-neutral number density ratio is larger than 10^{-3} . We therefore considered the impact of excitation by electrons in our coma model, and showed that this process plays an important role in the rotational population of HF, with the largest impact observed at a distance of about 2000 km from the comet nucleus, a result of the jump in electron density.

The present results suggest that a non-LTE modelling of the excitation of HF and other molecular species in the cometary coma is required over a wide range of distance to the nucleus, and that accurate excitation rate coefficients are needed.

ACKNOWLEDGEMENTS

J.L. acknowledges support from Internal Funds KU Leuven through Grant No. 19-00313. F.L. acknowledges Rennes Metropole for financial support. This research was supported by the CNRS national program ‘Physique et Chimie du Milieu Interstellaire’. Nicolas Biver is acknowledged for useful discussions.

DATA AVAILABILITY

The data underlying this article are available in the article and in its online supplementary material.

REFERENCES

- Ayouz M., Faure A., Tennyson J., Tudorovskaya M., Kokoouline V., 2021, *Atoms*, 9, 62
- Balança C., Scribano Y., Loreau J., Lique F., Feautrier N., 2020, *Mon. Not. R. Astron. Soc.*, 495, 2524
- Bergman P., Lerner M. S., Olofsson A. O. H., Wirstrom E., Black J. H., Bjerkeli P., Parra R., Torstensson K., 2022, *A&A*, 660, A118
- Bockelée-Morvan D., 1987, *A&A*, 181, 169
- Bockelée-Morvan D. et al., 2014, *A&A*, 562, A5
- Bockelée-Morvan D., Crovisier J., Mumma M. J., Weaver H. A., 2004, *The composition of cometary volatiles, Comets II*, M. C. Festou, H. U. Keller, and H. A. Weaver (eds.), University of Arizona Press, Tucson, p.391-423
- Boursier C., Mandal B., Babikov D., Dubernet M. L., 2020, *Mon. Not. R. Astron. Soc.*, 498, 5489

- Buffa G., Tarrini O., Scappini F., Cecchi-Pestellini C., 2000, *ApJS*, 128, 597
- De Keyser J. et al., 2017, *Mon. Not. R. Astron. Soc.*, 469, S695
- Desrousseaux B., Lique F., 2018, *Mon. Not. R. Astron. Soc.*, 476, 4719
- Dhooghe F. et al., 2017, *Mon. Not. R. Astron. Soc.*, 472, 1336
- Dubernet M. L., Quintas-Sánchez E., 2019, *Molecular Astrophysics*, 16, 100046
- Emprechtinger M., Monje R. R., van der Tak F. F. S., van der Wiel M. H. D., Lis D. C., Neufeld D., Phillips T. G., Ceccarelli C., 2012, *Ap. J.*, 756, 136
- Faure A., Lique F., Loreau J., 2020, *Mon. Not. R. Astron. Soc.*, 493, 776
- Faure A., Lique F., Loreau J., 2022, in *ECLA2020 proceedings* (submitted), Springer Nature, Eds. V. Mennella and C. Joblin, ed.
- Gordon I. E. et al., 2017, *J. Quant. Spec. Radiat. Transf.*, 203, 3
- Green S., 1993, *ApJ*, 412, 436
- Guillon G., Stoecklin T., 2012, *Mon. Not. R. Astron. Soc.*, 420, 579
- Huebner W. F., Mukherjee J., 2015, *Planet. Space Sci.*, 106, 11
- Itikawa Y., 1972, *Journal of the Physical Society of Japan*, 32, 217
- Itikawa Y., 2017, *Journal of Physical and Chemical Reference Data*, 46, 013105
- Konings M., Desrousseaux B., Lique F., Loreau J., 2021, *The Journal of Chemical Physics*, 155, 104302
- Kyrö E., 1981, *Journal of Molecular Spectroscopy*, 88, 167
- Loreau J., Faure A., Lique F., 2018, *J. Chem. Phys.*, 148, 244308
- Loreau J., Kalugina Y. N., Faure A., van der Avoird A., Lique F., 2020, *J. Chem. Phys.*, 153, 214301
- Loreau J., Lique F., Faure A., 2018, *Ap. J. Lett.*, 853, L5
- Neufeld D. A., Wolfire M. G., 2009, *Ap. J.*, 706, 1594
- Phillips T. G. et al., 2010, *A&A*, 518, L109
- Quack M., Troe J., 1975, *Ber. Bunsenges. Phys. Chem.*, 79, 170
- Reese, C., Stoecklin, T., Voronin, A., Rayez, J. C., 2005, *A&A*, 430, 1139
- Rohr K., Linder F., 1976, *Journal of Physics B Atomic Molecular Physics*, 9, 2521
- Thummel H. T., Nesbet R. K., Peyerimhoff S. D., 1992, *Journal of Physics B Atomic Molecular Physics*, 25, 4553
- Viglaska D., Wang X.-G., Carrington T., Tew D. P., 2022, *Journal of Molecular Spectroscopy*, 384, 111587
- Webb D. U., Narahari Rao K., 1968, *Journal of Molecular Spectroscopy*, 28, 121
- Xie X., Mumma M. J., 1992, *ApJ*, 386, 720
- Zakharov V., Bockelée-Morvan D., Biver N., Crovisier J., Lecacheux A., 2007, *A&A*, 473, 303

APPENDIX A: VALIDATION OF THE TIME-INDEPENDENT MODEL

In our steady-state non-LTE model, the H₂O density profile follows a simple Haser model, as shown in Fig. A1, with a uniform gas kinetic temperature of 50 K. The electron and

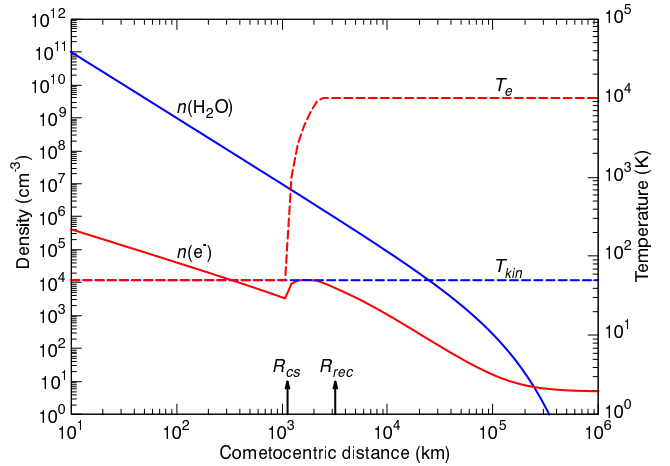


Figure A1. Coma density (solid lines) and temperature (dashed lines) profiles of H₂O (blue) and electrons (red) used in our non-LTE model. See text for details.

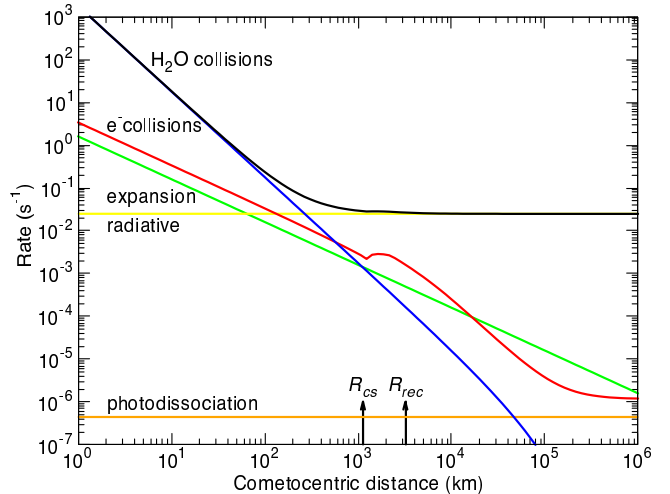


Figure A2. The different rates (in s⁻¹) for the processes involved in the depopulation of the HF level $j = 1$ as functions of the cometocentric distance. The black solid line denotes the sum of collisional and radiative rates.

density temperature profiles were taken from the model of Zakharov et al. (2007) where full details can be found.

In order to assess the validity of the steady-state assumption to solve the SE equations, we plot in Fig. A2 the different rates involved in the depopulation of the HF $j_2 = 1$ level: collisional de-excitation by H₂O molecule and electrons (present data), spontaneous emission and infrared pumping (data taken from HITRAN database), coma expansion ($\gamma = 2v_{exp}/R$ with $v_{exp}=0.8$ km.s⁻¹) and photodissociation ($\beta = 4.4 \times 10^{-7}$ s⁻¹ from Huebner & Mukherjee (2015)). The black solid line denotes the sum of collisional and radiative rates. Note that the contribution of IR pumping is negligible. It can be observed that the photodissociation and expansion processes both have minor contributions at all cometocentric distances so that the standard steady-state approximation of SE should be reliable over the entire coma.

It should be noted that similar results were recently ob-

served by Bergman et al. (2022) in the case of HCN. By running time-dependent radiative transfer calculations, these authors were able to quantify these effects and they have shown that the photodissociation and expansion processes do actually modify the HCN level populations by less than 15%. Even smaller deviations are expected in the case of HF since its spontaneous emission rates are much larger than those of HCN. More generally, photochemical and time-dependent effects should be moderate for molecules with sizeable dipole moments owing to their large radiative rates and large electron-impact excitation rate coefficients. The steady-state assumption may become questionable for molecules with small dipoles (e.g. CO) or for comets with small water production rates (or small electron density).